Available online at www.sciencedirect.com
SCIENCE DIRECT®
Comput. Methods Appl. Mech. Engrg. 194 (2005) 1057–1074
Computer methods in applied mechanics and engineering
www.elsevier.com/locate/cma

A semi-analytical algorithm for the evaluation of the nearly singular integrals in three-dimensional boundary element methods

Zhongrong Niu [a,*], W.L. Wendland [b], Xiuxi Wang [c], Huanlin Zhou [a]

[a] *Department of Engineering Mechanics, Hefei University of Technology, Hefei 230009, PR China*
[b] *Mathematisches Institut A, Stuttgart University, Pfaffenwaldring 57, 70569 Stuttgart, Germany*
[c] *Department of Mechanics, University of Science and Technology of China, Hefei 230026, PR China*

Received 22 April 2003; received in revised form 25 November 2003; accepted 7 June 2004

Abstract

The nearly singular integrals occur in the boundary integral equations when the source point is close to an integration element (as compared to its size) but not on the element. In this paper, the concept of a relative distance from a source point to the boundary element is introduced to describe possible influence of the singularity of the integrals. Then a semi-analytical algorithm is proposed for evaluating the nearly strongly singular and hypersingular integrals in the three-dimensional BEM. By using integration by parts, the nearly singular surface integrals on the elements are transformed to a series of line integrals along the contour of the element. The singular behavior, which appears as factor, is separated from remaining regular integrals. Consequently standard numerical quadrature can provide very accurate evaluation of the resulting line integrals. The semi-analytical algorithm is applied to analyzing the three-dimensional elasticity problems, such as very thin-walled structures. Meanwhile, the displacements and stresses at the interior points very close to its bounding surface are also determined efficiently. The results of the numerical investigation demonstrate the accuracy and effectiveness of the algorithm.

Keywords: Boundary element method; Nearly singular integral; Regularization; Elasticity; Three-dimensions

* Corresponding author. Tel.: +86 551 2901437; fax: +86 551 2902066.
E-mail address: niuzhong@mail.hf.ah.cn (Z. Niu).

0045-7825/$ - see front matter © 2004 Elsevier B.V. All rights reserved.
doi:10.1016/j.cma.2004.06.024

1. Introduction

The calculation of potentials, fluxes, displacements and stresses on and near the boundary is one of major interest problems in boundary element analyses. Experience has shown that the boundary element methods (BEM) have advantages over other numerical methods for involving high gradients of field quantities. The effectiveness of the BEM depends on a number of factors, such as mesh distribution, element choice and accuracy of element integrals. However, the boundary integral equations (BIE) usually contain singular integrals whose evaluation is difficult although the original problems are not singular. It seems that this is the price, BEM has to pay for the reduction of dimensions. In fact, it is the singularity that ensures stability and accuracy for the solutions of the BEM.

Currently, the algorithms for calculating singular integrals in the BEM can be categorized as follows [23]: regularization methods before or after the discretization of the BIE. The former reduces the singular order of the integrals by the use of the Stokes or the Gaussian theorem [9,22]. In the second category, the divergent parts of singular integrals are eliminated by using semi-analytical or analytical way in the intrinsic coordinate system for every singular element [10,11,8]. In Ref. [12], strongly singular and hypersingular surface integrals are reduced to weakly singular ones by analytic regularization. Then these weakly singular integrals are treated with Gaussian product rules after introducing polar coordinates. Reviews on the treatment about some singular integrals can be seen in Refs. [23,3]. When a load point approaches the boundary, it is a limiting procedure that the distance r between the source point and the field point tends to zero. Some methods [10,11] have efficiently calculated the singular integrals when the kernel functions are Hölder continuous by means of the limiting analysis. However, for $r \neq 0$, the quadrature methods established by earlier studies are not efficient for calculating the interior quantities close to the boundary. The effect is usually referred to as the ''boundary layer effect''. This is the nearly singular integral.

In BEM, nearly singular integrals come up in the following cases: (1) Computing the interior quantities close to the boundary; (2) There are great differences among the sizes of adjoining element meshes; (3) For narrow and thin domains; (4) For non-linear problems in which the integrals in the domains near the boundary need to be calculated. Because of the difficulty of evaluating the nearly singular integrals, for a long time there has existed an opinion that the BEM are not suitable for analyzing thin-body problems.

It is well known that rigid body translations [4,14] can be used for regularizing the Cauchy principal value integrals. According to this idea, a particular solution field method is developed [1,24]. The method employs the uniform or first order stress fields approximately to imitate the unknown stress fields in the elasticity, which indirectly evaluates the nearly hypersingular integrals. However, as the gradients of field functions get large, the method produces large deviations. By utilizing the quantity at the closest point on the boundary to the load point, Liu [15] proposes a strategy that the nearly singular integral is dealt with by adding and subtracting a term in the BIE. It follows that the strongly singular integral can be transformed into line integrals by the Stokes' theorem. The treatment makes that the three-dimensional BEM can successfully analyze shell-like structures. In Ref. [18], an analytical scheme is given to linear triangular elements, which is applied for calculating Cauchy principal value and nearly strongly singular integrals in three-dimensional elasticity. After then, Davey et al. [6] develop a semi-analytical integration scheme to linear triangular elements for a kind of the singular integrals in steady-state elastodynamic problems. The scheme adopts the subtraction way to formulate the integrals into singular and non-singular parts based on the Taylor expansions. The singular part is computed analytically. Wendland et al. [25] obtain the higher order derivatives of the primary field function $u(\boldsymbol{x})$ on the boundary with an extraction technique in the BEM. Then, for the load point $\boldsymbol{y}$ sufficiently close to the boundary, constructing the Taylor series expansion on the local surface near $\boldsymbol{y}$ determines the interior quantities. Based on the standard boundary contour method (BCM) [21] and boundary node method (BNM) [19], by the use of the continuous displacement and stress BIEs [5], Mukherjee et al. [20] propose an efficient approach, called new BCM and new BNM, in order to evaluate the displacements and stresses at points inside a bulky solid body that lie close

to its bounding surface. The method is only implemented after all the displacements and tractions on the surface of the body are obtained. For a long time, most of current numerical methods, including finite element method, have been difficult to analyze very thin structures, such as the problems of thin coatings and their interfacial mechanics. Recently, many efforts on the evaluation of the nearly singular integrals make that the BEM can deal with these difficult problems. Some applications of boundary element analyses for thin-body structures, especially for the two-dimensional problems, can be found in many literatures [2,13,16,17].

The present work proposes a new semi-analytical algorithm for evaluating the nearly strongly singular and hypersingular integrals on the triangular and quadrilateral elements in three-dimensional BEM. After the boundary integral equations are discretized on the boundary, the singular surface integrals on the element can be transformed into a series of line integrals by using integration by parts. Then the line integrals can efficiently be calculated by standard quadrature techniques. The semi-analytical algorithm is used to analyze three-dimensional elasticity problems.

2. The analysis of the nearly singular integrals in BEM

Here, we consider the boundary integral equations of linear elasticity. The displacements and stresses at any point $\boldsymbol{y}$ in the domain Ω are represented by

$$u_i(\boldsymbol{y}) = \int_\Gamma [U^*_{ij}(\boldsymbol{x},\boldsymbol{y})t_j(\boldsymbol{y}) - T^*_{ij}(\boldsymbol{x},\boldsymbol{y})u_j(\boldsymbol{x})]\,\mathrm{d}\Gamma + \int_\Omega U^*_{ij}b_j(\boldsymbol{x})\,\mathrm{d}\Omega, \tag{1}$$

$$\sigma_{ij}(\boldsymbol{y}) = \int_\Gamma [W^*_{ijk}(\boldsymbol{x},\boldsymbol{y})t_k(\boldsymbol{x}) - S^*_{ijk}(\boldsymbol{x},\boldsymbol{y})u_k(\boldsymbol{x})]\,\mathrm{d}\Gamma + \int_\Omega W^*_{ijk}b_k(\boldsymbol{x})\,\mathrm{d}\Omega, \tag{2}$$

where $i,j,k = 1,2,3$; $\Gamma = \partial\Omega$. Here and in what follows, the summation convention is used. $u_j(\boldsymbol{x})$, $t_j(\boldsymbol{x})$ are the displacement and traction on the boundary Γ, respectively. $b_j(\boldsymbol{x})$ is the body load. U^*_{ij} and T^*_{ij} are the Kelvin displacement and traction fundamental solutions, respectively. W^*_{ijk} and S^*_{ijk} are defined by derivatives of U^*_{ij} and T^*_{ij}, respectively, as follows:

$$[U^*_{ij}]_{3\mathrm{D}}(\boldsymbol{x},\boldsymbol{y}) = \frac{1}{16\pi(1-\nu)Gr}\left[(3-4\nu)\delta_{ij} + r_{,i}r_{,j}\right], \tag{3a}$$

$$[U^*_{ij}]_{2\mathrm{D}}(\boldsymbol{x},\boldsymbol{y}) = \frac{1}{8\pi(1-\nu)G}\left[(3-4\nu)\ln r\delta_{ij} - r_{,i}r_{,j}\right] \quad \text{(plane strain)}, \tag{3b}$$

$$T^*_{ij}(\boldsymbol{x},\boldsymbol{y}) = \frac{1}{4\alpha\pi(1-\nu)r^\alpha}\left\{(1-2\nu)(r_{,i}n_{,j} - r_{,j}n_{,i}) - r_{,n}\left[(1-2\nu)\delta_{ij} + \beta r_{,i}r_{,j}\right]\right\}, \tag{4}$$

$$W^*_{ijk}(\boldsymbol{x},\boldsymbol{y}) = \frac{1}{4\alpha\pi(1-\nu)r^\alpha}\left[(1-2\nu)(r_{,j}\delta_{ik} + r_{,i}\delta_{kj} - r_{,k}\delta_{ji}) + \beta r_{,i}r_{,j}r_{,k}\right], \tag{5}$$

$$\begin{aligned} S^*_{ijk}(\boldsymbol{x},\boldsymbol{y}) = {} & \frac{G}{2\alpha\pi(1-\nu)r^\beta}\left\{\beta r_{,n}\left[(1-2\nu)r_{,k}\delta_{ji} + \nu(r_{,i}\delta_{jk} + r_{,j}\delta_{ik}) - \gamma r_{,i}r_{,j}r_{,k}\right]\right. \\ & \left. + (1-2\nu)(\beta r_{,i}r_{,k}n_{,j} + \delta_{jk}n_i + \delta_{ik}n_j) + \beta\nu(r_{,i}r_{,k}n_j + r_{,j}r_{,k}n_i) - (1-4\nu)\delta_{ji}n_k\right\}, \end{aligned} \tag{6}$$

where G is the shear modulus and ν the Poisson ratio. α, β, γ are coefficients with $\alpha = 1$, $\beta = 2$ and $\gamma = 4$ for two-dimensional problems, $\alpha = 2$, $\beta = 3$ and $\gamma = 5$ for three dimensions. $\boldsymbol{y}$ is the source or load point and $\boldsymbol{x}$

the field point on the closed surface Γ. Let y_i and x_i denote the Cartesian coordinate components of $\boldsymbol{y}$ and $\boldsymbol{x}$, respectively. n_i denotes the components of the outward unit normal at $\boldsymbol{x}$. Thus we can write

$$\left.\begin{aligned} r_i &= x_i - y_i, \quad r = \sqrt{r_i r_i} \\ r_{,i} &= \partial r/\partial x_i, \quad r_{,n} = \partial r/\partial n = r_{,i} n_i \end{aligned}\right\}. \tag{7}$$

Let $\boldsymbol{y}$ approach the boundary Γ in Eqs. (1) and (2). It follows the displacement boundary integral equation

$$C_{ij}(\boldsymbol{y}) u_j(\boldsymbol{y}) = \int_\Gamma U^*_{ij}(\boldsymbol{x},\boldsymbol{y}) t_j(\boldsymbol{x})\,\mathrm{d}\Gamma(\boldsymbol{x}) - \int_\Gamma T^*_{ij}(\boldsymbol{x},\boldsymbol{y}) u_j(\boldsymbol{x})\,\mathrm{d}\Gamma(\boldsymbol{x}) + \int_\Omega U^*_{ij} b_j\,\mathrm{d}\Omega. \tag{8}$$

If $t_k(\boldsymbol{x})$ and the partial derivatives of $u_k(\boldsymbol{x})$ satisfy the Hölder continuity near the point $\boldsymbol{x}$ on Γ, when $\boldsymbol{y} \to \boldsymbol{x}$, we can write the stress boundary integral equations

$$B_{ijst}(\boldsymbol{y}) \sigma_{st}(\boldsymbol{y}) = \int_\Gamma W^*_{ijk} t_k(\boldsymbol{x})\,\mathrm{d}\Gamma(\boldsymbol{x}) - \oint\!\!\!\!\!\!=_\Gamma S^*_{ijk} u_k(\boldsymbol{x})\,\mathrm{d}\Gamma(\boldsymbol{x}) + \int_\Omega W^*_{ijk} b_k\,\mathrm{d}\Omega, \tag{9}$$

where $\oint_\Gamma$ denotes the Cauchy principal value integral and $\oint\!\!\!\!\!\!=_\Gamma$ denotes the Hardamard finite part of the integral; $C_{ij}(\boldsymbol{y})$ and $B_{ijst}(\boldsymbol{y})$ are defined as the displacement and stress singular coefficients, respectively, which depend on the material parameters and the local geometry of Γ at $\boldsymbol{y}$. There are $C_{ij} = \delta_{ij}/2$ at a smooth boundary point and $B_{ijst}(\boldsymbol{y}) = \delta_{ij}\delta_{st}/2$ at a smooth boundary point and t_k is continuous at the point. The conventional BEM in the elasticity problems obtains the boundary displacements and tractions by solving Eq. (8). Then all of the displacements and stresses at the interior points can be determined by Eqs. (1) and (2). In the ways, when $r \to 0$, these kernel functions in the BIE present the singularity to a different extent. U^*_{ij} shows a weak singularity of order $1/r$ for three-dimensional problems and $\ln r$ for two-dimensional problems; T^*_{ij} and W^*_{ijk} have a strong singularity of order $1/r^{\beta-1}$; S^*_{ijk} has a hypersingularity of order $1/r^{\beta}$. When the source point $\boldsymbol{y}$ is not on the boundary but close to the boundary, the singularity leads to nearly singular integrals in Eqs. (1) and (2) so that the evaluation of the conventional numerical quadrature is invalid on the elements close to the source point $\boldsymbol{y}$.

In the boundary element analysis based on Eq. (8), consider flat triangular element Γ_e close to the source point $\boldsymbol{y}$ (y_1, y_2, y_3) with three nodes, as shown in Fig. 1. A local coordinate system $o\xi\eta$ is defined on Γ_e with the origin being node 1, as shown in Fig. 2. The element Γ_e is made a linear isoparametric element. According to the collocation scheme, the geometry, displacements and tractions on Γ_e are described by linear shape functions in the local system $o\xi\eta$ as

$$x_i = N_m(\xi,\eta) x_{mi}, \quad m = 1,2,3, \tag{10}$$

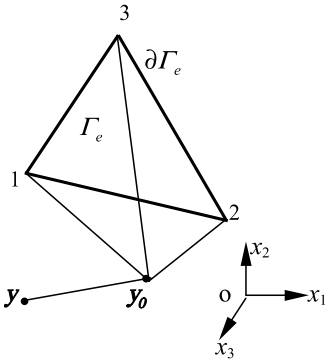

Fig. 1. Point $\boldsymbol{y}$ and the element Γ_e.

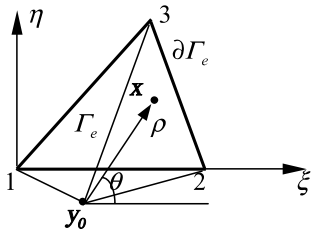

Fig. 2. The local systems $\xi\eta$ and $\rho\theta$.

$$u_i = N_m(\xi,\eta)u_{mi}, \tag{11}$$

$$t_i = N_m(\xi,\eta)t_{mi}, \tag{12}$$

where

$$N_m(\xi,\eta) = \frac{1}{2A}(a_m + b_m\xi + c_m\eta), \tag{13}$$

$$a_1 = \xi_2\eta_3 - \xi_3\eta_2, \quad a_2 = \xi_3\eta_1 - \xi_1\eta_3, \quad a_3 = \xi_1\eta_2 - \xi_2\eta_1,$$

$$b_1 = \eta_2 - \eta_3, \quad b_2 = \eta_3 - \eta_1, \quad b_3 = \eta_1 - \eta_2,$$

$$c_1 = \xi_3 - \xi_2, \quad c_2 = \xi_1 - \xi_3, \quad c_3 = \xi_2 - \xi_1,$$

x_{mi}, u_{mi} and t_{mi} are the coordinate, displacement and traction at node m along the x_i-direction on Γ_e, respectively. A is the area of Γ_e. ξ_m and η_m are the coordinates of node m in the coordinate system $o\xi\eta$, which are determined by x_{mi}. The Jacobian of the mapping from the coordinate $ox_1x_2x_3$ to $o\xi\eta$ on Γ_e is obtained as

$$J^s = \frac{\partial(x_1,x_2,x_3)}{\partial(\xi,\eta)} = \left[\left(\frac{\partial(x_2,x_3)}{\partial(\xi,\eta)}\right)^2 + \left(\frac{\partial(x_3,x_1)}{\partial(\xi,\eta)}\right)^2 + \left(\frac{\partial(x_1,x_2)}{\partial(\xi,\eta)}\right)^2\right]^{1/2} = 1, \tag{14}$$

since the relation of the transformation is linear. The perpendicular point $\boldsymbol{y}_0(\xi_0,\eta_0)$ of $\boldsymbol{y}$ in the plane of Γ_e can easily be determined. Then, we define a polar coordinate system $\rho\theta$ in the plane $\xi\eta$. The pole and polar axis of the system coincide with the point (ξ_0,η_0) and the parallel line of the axis ξ, respectively, as seen in Fig. 2. One performs the coordinate transformation

$$\xi - \xi_0 = \rho\cos\theta, \quad \eta - \eta_0 = \rho\sin\theta. \tag{15}$$

The transformation Jacobian is

$$J^\rho = \frac{\partial(\xi,\eta)}{\partial(\rho,\theta)} = \rho. \tag{16}$$

Substituting Eq. (15) into Eqs. (10) and (13) yields

$$N_m(\xi,\eta) = \frac{1}{2A}\rho(b_m\cos\theta + c_m\sin\theta) + N_m(\xi_0,\eta_0),$$

$$x_i = \frac{1}{2A}\rho(b_m\cos\theta + c_m\sin\theta)x_{mi} + y_{0i}, \tag{17}$$

where

$$y_{0i} = N_m(\xi_0,\eta_0)x_{mi} \tag{18}$$

are the coordinates of the point $\boldsymbol{y}_0$ in the system $ox_1x_2x_3$. By introducing Eq. (17) into Eq. (7), there are

$$x_i - y_i = r_i = \frac{1}{2A}\rho(b_m \cos\theta + c_m \sin\theta)x_{mi} + y_{0i} - y_i \tag{19}$$

and

$$R = r^2 = \rho^2 + \delta_1^2, \tag{20}$$

where

$$\delta_1^2 = (y_{0i} - y_i)(y_{0i} - y_i), \tag{21}$$

δ_1 is the perpendicular distance from the source point $\boldsymbol{y}$ to the plane of Γ_e. If the point $\boldsymbol{y}_0$ is outside of Γ_e but in the same plane as Γ_e, there exists a closest point on Γ_e to $\boldsymbol{y}_0$. Let δ_2 denote the distance from $\boldsymbol{y}_0$ to the closest point. Here we introduce the concept of relative distance according to

$$e_1 = \delta_1/L_{\max}, \quad e_2 = \delta_2/L_{\max}, \tag{22}$$

where $L_{\max}$ is maximum of the lengths of three edges of the element. When $\boldsymbol{y}_0$ gets close to Γ_e or in Γ_e, Eq. (20) shows that the measure of $1/r \to \infty$ depends on the extent of $e_1 \to 0$. Hence, e_1 is defined *relative distance* from the source point to the element Γ_e. In fact, $\sqrt{e_1^2 + e_2^2}$ can be termed a relative distance too. The integrals on Γ_e can be formulated in the polar coordinate system by

$$\mathrm{d}\Gamma(x) = J^s \,\mathrm{d}\xi \,\mathrm{d}\eta = \rho \,\mathrm{d}\rho \,\mathrm{d}\theta.$$

After substituting Eqs. (11)–(20) into Eqs. (1) and (2), the surface integrals on Γ_e in Eqs. (1) and (2) are described by the following integral types

$$I_n = \int_{\Gamma_e} \frac{1}{R^{n/2}} Q_n(\rho,\theta)\rho \,\mathrm{d}\rho \,\mathrm{d}\theta, \quad n = 1,3,5,7, \tag{23}$$

where R is a quadratic function of ρ, $Q_n(\rho,\theta)$ are polynomial functions with respect to ρ, $\cos\theta$ and $\sin\theta$, in which the orders of the polynomials are finite. If straightforward quadrature schemes are used to evaluate the integrals of Eq. (23), there leads to a tremendous loss of accuracy with the reduction of the relative distance e_1 and e_2. Therefore, small e_1 and e_2 are the main causes of the nearly singular integrals.

3. Formulations of the semi-analytical algorithm

The idea of the regularization for the nearly singular integrals is that the surface integrals Eq. (23) are transformed into line integrals along the contour of Γ_e by utilizing a series of integration by parts. In Eq. (23), the first step implements the integration with respect to the variable ρ, i.e.,

$$K_n(\rho,\theta) = \int \frac{1}{R^{n/2}} Q_n(\rho,\theta)\rho \,\mathrm{d}\rho. \tag{24}$$

Here the nearly singular integrals in Eq. (24) are categorized as two cases according to $e_1 \neq 0$ and $e_1 = 0$. For the integrals of the two cases, the formulations of the regularization are given, respectively, in the following.

Case 1. $e_1 \neq 0$

There exists the recurrence formula of the integral as

$$J_1 = \int \frac{\mathrm{d}\rho}{r} = \ln\left(\rho + \sqrt{\rho^2 + \delta_1^2}\right) + c,$$

$$J_n = \int \frac{\mathrm{d}\rho}{R^{n/2}} = \frac{\rho}{\delta_1^2(n-2)(\rho^2+\delta_1^2)^{n/2-1}} + \frac{n-3}{\delta_1^2(n-2)} \int \frac{\mathrm{d}\rho}{(\rho^2+\delta_1^2)^{n/2-1}} \quad (n \geqslant 3).$$

By means of the results above, one makes the integration by parts in Eq. (24). There is

$$K_n(\rho,\theta) = -\frac{Q_n}{(n-2)r^{n-2}} + \frac{1}{(n-2)} \int \frac{Q_n'}{r^{n-2}}\,\mathrm{d}\rho, \tag{25}$$

where $(\cdots)' = \mathrm{d}(\cdots)/\mathrm{d}\rho$. Then, the technique of the integration by parts is done over and over in Eq. (25). It produces the following formulations

$$\begin{aligned} K_1(\rho,\theta) = {} & rQ_1 - \frac{1}{2}Q_1'[\rho r + \delta_1^2 \ln(\rho+r)] + \frac{1}{2}Q_1''\left[\frac{1}{3}r^3 + \delta_1^2\rho\ln(\rho+r) - \delta_1^2 r\right] \\ & - \frac{1}{4}Q_1'''\left[\frac{1}{6}\rho r^3 - \frac{5}{4}\delta_1^2\rho r + \delta_1^2\rho^2\ln(\rho+r) - \frac{1}{4}\delta_1^4\ln(\rho+r)\right] \\ & + \frac{1}{4}\int Q_1^{(4)}\left[\frac{1}{6}\rho r^3 - \frac{5}{4}\delta_1^2\rho r + \delta_1^2\rho^2\ln(\rho+r) - \frac{1}{4}\delta_1^4\ln(\rho+r)\right]\mathrm{d}\rho, \end{aligned} \tag{26a}$$

$$\begin{aligned} K_3(\rho,\theta) = {} & \int \frac{\rho Q_3(\rho,\theta)}{r^3}\,\mathrm{d}\rho = -\frac{1}{r}Q_3 + Q_3'\ln(\rho+r) - Q_3''[\rho\ln(\rho+r) - r] \\ & + \frac{1}{4}Q_3'''[2\rho^2\ln(\rho+r) - \delta_1^2\ln(\rho+r) - 3\rho r] \\ & - \frac{1}{4}Q_3^{(4)}\left[-\frac{11}{9}r^3 + \frac{5}{3}\delta_1^2 r + \frac{2}{3}\rho^3\ln(\rho+r) - \delta_1^2\rho\ln(\rho+r)\right] \\ & + \frac{1}{4}\int Q_3^{(5)}\left[-\frac{11}{9}r^3 + \frac{5}{3}\delta_1^2 r + \frac{2}{3}\rho^3\ln(\rho+r) - \delta_1^2\rho\ln(\rho+r)\right]\mathrm{d}\rho., \end{aligned} \tag{26b}$$

$$\begin{aligned} K_5(\rho,\theta) = {} & \int \frac{\rho Q_5(\rho,\theta)}{r^5}\,\mathrm{d}\rho = -\frac{1}{3r^3}Q_5 + \frac{1}{6\delta_1^2}\left[\frac{1}{r}R'Q_5' - 2rQ_5''\right] \\ & + \frac{1}{6\delta_1^2}Q_5'''[\rho r + \delta_1^2\ln(\rho+r)] - \frac{1}{6\delta_1^2}Q_5^{(4)}\left[\frac{1}{3}r^3 + \delta_1^2\rho\ln(\rho+r) - \delta_1^2 r\right] \\ & + \frac{1}{12\delta_1^2}Q_5^{(5)}\left[\frac{1}{6}\rho r^3 - \frac{5}{4}\delta_1^2\rho r + \delta_1^2\rho^2\ln(\rho+r) - \frac{1}{4}\delta_1^4\ln(\rho+r)\right] \\ & - \frac{1}{12\delta_1^2}\int Q_5^{(6)}\left[\frac{1}{6}\rho r^3 - \frac{5}{4}\delta_1^2\rho r + \delta_1^2\rho^2\ln(\rho+r) - \frac{1}{4}\delta_1^4\ln(\rho+r)\right]\mathrm{d}\rho, \end{aligned} \tag{26c}$$

$$\begin{aligned} K_7(\rho,\theta) = {} & \int \frac{\rho Q_7(\rho,\theta)}{r^7}\,\mathrm{d}\rho = -\frac{1}{5r^5}Q_7(\rho,\theta) + \frac{\rho}{15\delta_1^2 r}Q_7'\left(\frac{1}{r^2} + \frac{2}{\delta_1^2}\right) - \frac{1}{15\delta_1^2}Q_7''\left[\frac{2r}{\delta_1^2} - \frac{1}{r}\right] \\ & + \frac{\rho}{15\delta_1^4}rQ_7''' - \frac{1}{45\delta_1^4}r^3Q_7^{(4)} + \frac{1}{360\delta_1^4}Q_7^{(5)}[2\rho r^3 + 3\delta_1^2\rho r + 3\delta_1^4\ln(\rho+r)] \\ & - \frac{1}{360\delta_1^4}Q_7^{(6)}\left[\frac{2}{5}r^3 + \delta_1^2 r^3 - 3\delta_1^4 r + 3\delta_1^4\rho\ln(\rho+r)\right] \\ & + \frac{1}{360\delta_1^4}\int Q_7^{(7)}\left[\frac{2}{5}r^3 + \delta_1^2 r^3 - 3\delta_1^4 r + 3\delta_1^4\rho\ln(\rho+r)\right]\mathrm{d}\rho. \end{aligned} \tag{26d}$$

Case 2. $e_1 = 0$, but $e_2 \neq 0$

It is termed the second kind of the nearly singular integrals. In the case, there is

$$r = \sqrt{\rho^2 + \delta_1^2} = \rho.$$

Eq. (24) can be written as

$$K_n(\rho,\theta) = \int \frac{1}{\rho^{n-1}} Q_n(\rho,\theta)\,\mathrm{d}\rho. \tag{27}$$

There exist the following integral formulas

$$\int \frac{1}{\rho^n}\,\mathrm{d}\rho = -\frac{1}{(n-1)\rho^{n-1}} + c, \quad n \neq 1,$$

$$\int \frac{1}{\rho}\,\mathrm{d}\rho = \ln\rho + c.$$

By the use of the above formulas, the integration by parts is again done for Eq. (27) by the similar way as above. We obtain

$$K_1(\rho,\theta) = \int Q_1(\rho,\theta)\,\mathrm{d}\rho = \rho Q_1 - \frac{1}{2}\rho^2 Q_1' + \frac{1}{6}\rho^3 Q_1'' - \frac{1}{24}\rho^4 Q_1''' + \frac{1}{24}\int \rho^4 Q_1^{(4)}\,\mathrm{d}\rho, \tag{28a}$$

$$\begin{aligned} K_3(\rho,\theta) &= \int \frac{1}{\rho^2} Q_3(\rho,\theta)\,\mathrm{d}\rho \\ &= -\frac{1}{\rho} Q_3 + \ln\rho Q_3' - \rho(\ln\rho - 1)Q_3'' + \frac{1}{2}\rho^2\left(\ln\rho - \frac{3}{2}\right)Q_3''' \\ &\quad - \frac{1}{6}\rho^3\left(\ln\rho - \frac{11}{6}\right)Q_3^{(4)} + \frac{1}{6}\int \rho^3\left(\ln\rho - \frac{11}{6}\right)Q_3^{(5)}\,\mathrm{d}\rho, \end{aligned} \tag{28b}$$

$$\begin{aligned} K_5(\rho,\theta) &= \int \frac{1}{\rho^4} Q_5(\rho,\theta)\,\mathrm{d}\rho \\ &= -\frac{1}{3\rho^3} Q_5 - \frac{1}{6\rho^2} Q_5' - \frac{1}{6\rho} Q_5'' + \frac{1}{6}\ln\rho Q_5''' - \frac{1}{6}\rho(\ln\rho - 1)Q_5^{(4)} \\ &\quad + \frac{1}{12}\rho^2\left(\ln\rho - \frac{3}{2}\right)Q_5^{(5)} - \frac{1}{12}\int \rho^2\left(\ln\rho - \frac{3}{2}\right)Q_5^{(6)}\,\mathrm{d}\rho, \end{aligned} \tag{28c}$$

$$\begin{aligned} K_7(\rho,\theta) &= \int \frac{1}{\rho^6} Q_7(\rho,\theta)\,\mathrm{d}\rho \\ &= -\frac{1}{5\rho^5} Q_7 - \frac{1}{20\rho^4} Q_7' - \frac{1}{60\rho^3} Q_7'' - \frac{1}{120\rho^2} Q_7''' - \frac{1}{120\rho} Q_7^{(4)} + \frac{1}{120}\ln\rho Q_7^{(5)} \\ &\quad - \frac{1}{120}\rho(\ln\rho - 1)Q_7^{(6)} + \frac{1}{120}\int \rho(\ln\rho - 1)Q_7^{(7)}\,\mathrm{d}\rho. \end{aligned} \tag{28d}$$

For Eq. (23) the orders of the polynomials $Q_n(\rho,\theta)$ ($n = 1, 3, 5, 7$) with respect to ρ are always finite after the BIE is discretized. If the linear isoparametric triangular elements are adopted in the BIE of three-dimensional elasticity, there are certainly

$$Q_1'''(\rho,\theta) = 0, \quad Q_3^{(4)}(\rho,\theta) = 0, \quad Q_5^{(5)}(\rho,\theta) = 0, \quad Q_7^{(6)}(\rho,\theta) = 0. \tag{29}$$

If the quadratic sub-parametric flat elements are adopted, where the field quantities are modeled by the quadratic shape function, it results in

$$Q_1^{(4)}(\rho,\theta)=0,\quad Q_3^{(5)}(\rho,\theta)=0,\quad Q_5^{(6)}(\rho,\theta)=0,\quad Q_7^{(7)}(\rho,\theta)=0. \tag{30}$$

Consequently each of the last terms in Eqs. (26) and (28) will be zero. Hence the integrals $K_n(\rho,\theta)$ with respect to ρ have been integrated analytically. Then substituting Eqs. (26) or (28) into Eq. (23), one obtains

$$I_n=\int_{\partial\Gamma_e}[K_n(\rho,\theta)]_{\rho=\rho_1(\theta)}^{\rho_2(\theta)}\,\mathrm{d}\theta, \tag{31}$$

where $\partial\Gamma_e$ is the contour of element Γ_e. Noting Eq. (15) and Fig. 2, the representations of three edges of the triangular element in polar system $\rho\theta$ are

(1) Edge $\overline{12}$

$$\rho_{12}(\theta)=-\frac{\eta_0}{\sin\theta}. \tag{32a}$$

(2) Edge $\overline{23}$

$$\rho_{23}(\theta)=\frac{(\xi_2-\xi_0)\eta_3-(\xi_2-\xi_3)\eta_0}{\cos\theta\eta_3+(\xi_2-\xi_3)\sin\theta}. \tag{32b}$$

(3) Edge $\overline{31}$

$$\rho_{31}(\theta)=\frac{\xi_3\eta_0-\xi_0\eta_3}{\eta_3\cos\theta-\xi_3\sin\theta}. \tag{32c}$$

Thus, lower and upper bounds of the integration $K_n(\rho,\theta)$ with respect to ρ are taken from Eqs. (32a)–(32c), in turn. It can be seen that I_n are replaced by the line integrals with respect to the variable θ along the contour of Γ_e. Furthermore, the factor e_1 (or δ_1) led to the nearly singular integrals has been removed out of the integrants of the line integrals in Eqs. (31). Therefore the standard numerical quadrature scheme can achieve satisfactory results for the line integrals in the cases of very small e_1 and e_2.

Example 1. The evaluation of the surface integrals

$$I_{51}=\int\int_{\Gamma}\frac{1}{r^5}\,\mathrm{d}\Gamma(\boldsymbol{x}),\quad I_{71}=\mathrm{d}\Gamma(\boldsymbol{x}), \tag{a}$$

$$r=\{|\boldsymbol{x}-\boldsymbol{y}|,\boldsymbol{x}\in\Gamma\},\quad \boldsymbol{y}=(\Delta_2,\Delta_2,\Delta_1),$$

Γ is a triangular domain which is constructed by three points $(0,0,0)$, $(1,0,0)$ and $(1,1,0)$ as shown in Fig. 3. As the point $\boldsymbol{y}$ is close to Γ, one has $r\to 0$ so that the nearly singular integrals occur in Eq. (a).

Two approximate ways are employed to determine the integrals. The first way is directly to calculate the surface integrals with the conventional Gaussian quadrature according to the following step (see Fig. 2)

$$\int\int_{\Delta_{123}}(\cdots)\,\mathrm{d}\Gamma=\pm\int\int_{\Delta_{y_0}12}\pm\int\int_{\Delta_{y_0}23}\pm\int\int_{\Delta_{y_0}31}(\cdots)\,\mathrm{d}\Gamma,$$

where plus is taken when points y_0, 1 and 2 are anticlockwise ranked along the boundary of $\Delta_{y_0}12$, otherwise minus is taken. The others are same convention. The domain of each sub-triangle is transformed to the rectangle by using the so-called Duffy triangular coordinates [7]. Then the transformed integrals are computed by the 8×8-point Gaussian quadrature. The second way is the semi-analytical algorithm in which the

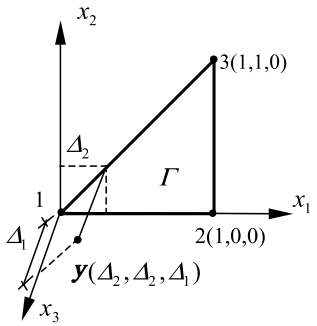

Fig. 3. The triangular domain Γ.

Table 1
The results of Example 1

Point $\boldsymbol{y}$		I_{51}			I_{71}		
Δ_1	Δ_2	Exact solution	Error of conventional	Error of semi-analytical	Exact solution	Error of conventional	Error of semi-analytical
0.001	0.01	0.10468e+10	−0.260e+02	0.461e−11	0.628e+15	−0.259e+02	0.190e−10
	0.1	0.10472e+10	−0.754e+02	0.342e−13	0.628e+15	−0.931e+02	0.199e−13
	0.6	0.10472e+10	−0.993e+02	0	0.628e+15	−1.000e+02	0
0.01	0.01	0.874e+06	−0.162e+02	−0.480e−04	0.583e+10	−0.228e+02	0.949e−04
	0.1	0.105e+07	−0.106e+02	−0.476e−11	0.628e+10	−0.209e+02	0.120e−10
	0.6	0.105e+07	0.264e+02	0.556e−13	0.628e+10	−0.416e+00	0.303e−13
0.1	0.01	0.333e+03	−0.254e+01	0.293e+00	0.215e+05	−0.430e+01	−0.540e−01
	0.1	0.873e+03	−0.912e+00	−0.207e−04	0.583e+05	−0.177e+01	0.150e−04
	0.6	0.104e+04	0.758e−01	0.369e−10	0.628e+05	−0.180e+00	−0.427e−10

resulting line integrals Eq. (31) instead of Eq. (a) are calculated. Here we take the 8-point Gaussian integration for each line integral. The errors of the evaluation are shown in Table 1 where *error* means

$$\text{error} = \frac{I_{\text{approx.}} - I_{\text{exact}}}{I_{\text{exact}}} \times 100\%.$$

The simple example is designed to test the accuracy of the semi-analytical algorithm. It is seen that the results obtained by using the semi-analytical algorithm are excellent agreement with the exact solution although the Δ_1 gets very small, however the ones of the conventional way are out of true when $\Delta_1 < 0.1$.

4. Numerical examples

In the section, the semi-analytical algorithm developed for the evaluation of the nearly singular integrals is used to determine the displacements and stresses of three-dimensional elasticity in the BEM. The conventional numerical quadrature is sufficient enough to evaluate the integrals on the elements far to the source point. The semi-analytical algorithm is available to the triangular elements. By the substitution of Eqs. (10), (13)–(20) into Eqs. (3)–(6) for a linear isoparametric triangular element Γ_e, one can write

$$U_{ij}^{*}=\frac{1}{16\pi(1-v)Gr}\left[(3-4v)\delta_{ij}+\frac{r_i r_j}{r^2}\right], \tag{33a}$$

$$T_{ij}^{*}=-\frac{1}{8\pi(1-v)r^3}\left\{\left[(1-2v)\delta_{ij}+3\frac{r_i r_j}{r^2}\right]n_l r_l+(1-2v)(n_i r_j-n_j r_i)\right\}, \tag{33b}$$

$$W_{ijk}^{*}=\frac{1}{8\pi(1-v)r^3}\left[(1-2v)(r_i\delta_{jk}+r_j\delta_{ik}-r_k\delta_{ij})+\frac{3}{r^2}r_i r_j r_k\right], \tag{33c}$$

$$\begin{aligned}S_{ijk}^{*}=&\frac{G}{4\pi(1-v)r^3}\left\{\frac{3r_l n_l}{r^2}\left[(1-2v)r_{,k}\delta_{ij}+v(r_i\delta_{jk}+r_j\delta_{ik})-\frac{5}{r^2}r_i r_j r_k\right]\right.\\&\left.+\frac{3v}{r^2}(n_i r_j+n_j r_i)r_k+(1-2v)\left(\frac{3n_k r_i r_j}{r^2}+n_i\delta_{jk}+n_j\delta_{ik}\right)-(1-4v)n_k\delta_{ij}\right\},\end{aligned} \tag{33d}$$

where r is the square root of a quadratic function of ρ. Then Eqs. (11), (12) and (33) are introduced into Eqs. (1) and (2) according to the collocation approach. Thus, in the boundary integral equation Eqs. (1) and (2), the surface integrals on Γ_e become the modes described by Eq. (23). Here r_i and N_m as seen in Eqs. (17) and (19) are linear functions of ρ. Hence it is easily verified that the conclusions of Eqs. (29) corresponding to the integrals on Γ_e exist. Now, with the semi-analytical algorithm we can calculate the resulting line integrals instead of the surface integrals on Γ_e if the integrals are nearly singular.

Generally the quadratic isoparametric elements with 8 nodes are appreciated because of the higher accuracy in three-dimensional BEM. As the nearly singular integrals occur in the elements, the straightforward evaluation using the conventional quadrature algorithms in Eqs. (1) and (2) results in a degeneracy of accuracy even if a large number of integral points are taken. Here, the calculation for a quadratic element Γ_8 can be improved by subdividing it into several triangular elements only when we need to compute its nearly singular integrals. Linear trial functions are used to describe the geometry, displacements and tractions on each of the triangular elements. In the other steps of analyzing the problem, Γ_8 still maintains the original quadratic element. A way of subdividing the element is seen in Fig. 4. Find the center point C in Γ_8 by

$$x_{Ci}=\sum_{m=1}^{8}N_m(\xi,\eta)x_{mi}|_{\xi=0,\eta=0},$$

where $N_m(\xi,\eta)$ $(m=1,2,\ldots,8)$ are quadratic shape functions. Make the displacements and tractions at point C be

$$u_{Ci}=\sum_{m=1}^{8}N_m(0,0)u_{mi},$$

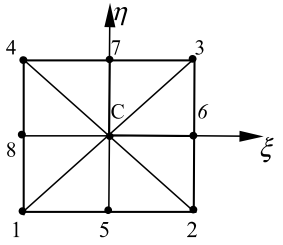

Fig. 4. The subdivision on Γ_8.

$$t_{Ci} = \sum_{m=1}^{8} N_m(0,0) t_{mi}.$$

Then Γ_8 can be replaced with the eight triangular elements constituted by each adjoining two nodes of the eight nodes and point C in turn. Thus the nearly singular integrals on these triangular elements can be calculated with the semi-analytical algorithm. The sum of these integrals on all of the eight triangular elements can supplant the original integrals on Γ_8. Note that the subdivision of Γ_8 and the extra computational time added by the strategy are not involved in the other procedures of the boundary element analysis. The following three examples are presented to demonstrate the effectiveness of the method. Here, eight-point Gaussian integration is used unless specified otherwise when the numerical integrals are done.

Example 2 (Bending of a cuboid beam). The beam is subjected to a pair of symmetrical linear distribution load $p_{\max} = 10$ MPa at its two ends. For the material, Young's modulus is $E = 210$ GPa and Poisson's ratio $v = 0.3$. Due to symmetry, we only need to consider the half of the beam. Its dimensions are shown in Fig. 5.

In the BEM model, the boundary is discretized by 24 quadratic elements with 74 nodes, where each of the six surfaces of the beam has four elements. The displacements and stresses in the interior domain close to point $A(5, 10, 10)$ are calculated by using the conventional method and the semi-analytical method. The conventional method is directly to compute the integrals in Eqs. (1) and (2) according to the quadratic elements by the standard Gaussian quadrature. In the semi-analytical algorithm, the nearly strongly singular and hypersingular integrals are computed according to the line integrals Eq. (31) on the refined triangular elements proposed in Fig. 4. The results are shown in Tables 2 and 3. u_1 is the displacement in the x_1-direction, σ_{11} the normal stress in the x_1-direction.

Here, for a quadratic element, the meaning of the relative distance e_1 is

$$e_1 = \delta / L_{\max},$$

where δ is the perpendicular distance from the source point to the element, $L_{\max}$ is the maximum of the lengths of the two diagonal lines of each quadrilateral element. The relative distance e_1 in every last column of the Tables 2 and 3 is the minimum for all elements corresponding to each load point. Here, the BE analysis for this simple problem obtains exact boundary displacements and tractions. Thus, the errors of the evaluation of the displacements and stresses at the interior points are all from the numerical quadrature for the BIEs (1) and (2). It can be seen that the semi-analytical method achieves more accurate results than

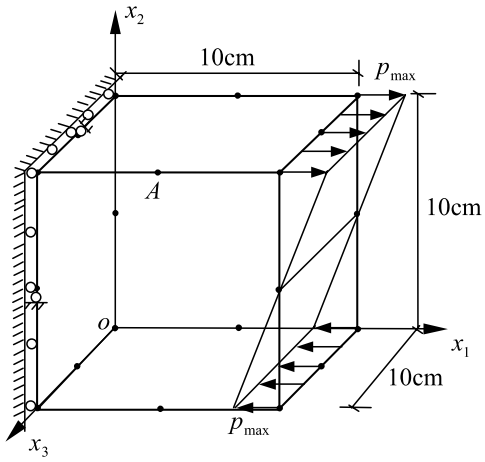

Fig. 5. Bending of the cuboid beam.

Table 2
The displacement u_1 ($\times 10^{-3}$ cm) of the cuboid beam

Point no.	Coordinates			Exact solution	Conventional solution	Semi-analytical solution	Relative distance e_1
	x_1 (cm)	x_2 (cm)	x_3 (cm)				
1	5.00	9.00	9.00	0.190476	0.19045	0.19048	0.1414
2	5.00	9.30	9.30	0.204762	0.20656	0.20477	0.09900
3	5.00	9.60.	9.60	0.219048	0.20075	0.21904	0.05657
4	5.00	9.90	9.90	0.233333	0.34617	0.23327	0.01414
5	5.00	9.92	9.92	0.234286	×	0.23421	0.01131
10	5.00	9.99	9.99	0.237619	×	0.23756	0.001414
12	5.00	9.999	9.999	0.238048	×	0.23802	0.000141
13	5.00	9.9999	9.9999	0.238091	×	0.23807	0.0000141
14	5.00	9.99999	9.99999	0.238095	×	0.23808	0.00000141

Table 3
The stress σ_{11} (MPa) of the cuboid beam

Point no.	Coordinates			Exact solution	Conventional solution	Semi-analytical solution	Relative distance e_1
	x_1 (cm)	x_2 (cm)	x_3 (cm)				
1	5.00	9.00	9.00	8.0000	7.8633	7.8000	0.1414
2	5.00	9.30	9.30	8.6000	9.9568	8.2659	0.0990
3	5.00	9.60.	9.60	9.2000	12.897	8.7017	0.0566
4	5.00	9.90	9.90	9.8000	×	9.2444	0.0141
5	5.00	9.92	9.92	9.8400	×	9.3104	0.0113
6	5.00	9.94	9.94	9.8800	×	9.3951	0.00849
7	5.00	9.96	9.96	9.9200	×	9.5193	0.00566
8	5.00	9.97	9.97	9.9400	×	9.6154	0.00424
9	5.00	9.98	9.98	9.9600	×	9.7705	0.00283
10	5.00	9.99	9.99	9.9800	×	10.130	0.00141
11	5.00	9.993	9.993	9.9860	×	10.392	0.00099

the conventional method, and is available to compute the quantities at the interior points very close to the boundary.

Example 3 (A hollow sphere subjected to internal pressure p on the inner surface). The inner radius of the hollow sphere is $a = 1$, outer radius $b = 4$, the applied load $p = 1$, material parameters $E = 1$, $v = 0.25$. Here and in what follows, assume that the relative units are all compatible.

Due to symmetry conditions, only one-eighth of the hollow sphere is considered in the BEM analysis, as shown in Fig. 6. Both inner and outer surfaces in one octant are discretized, respectively, with 27 and 65 eight-node quadrilateral elements (a total of 92 elements). The conventional method and the semi-analytical algorithm are used to calculate the displacements and stresses in the interior points of the vessel, where the relative distance e_1 is the same meaning as example 2. The radial displacement u_r, radial stress σ_{rr} and hoop stresses $\sigma_{\theta\theta}$ as functions of radius are shown in Fig. 7 and Table 4, respectively, together with exact solution and the results of the new BNM [20]. The new BNM is proposed to calculate the nearly singular integrals by Mukherjee et al. The new BNM takes 72 quadratic T6 triangles on each surface of the hollow sphere for the example, which obtains more accurate values than the standard BNM [19]. Meanwhile, Ref. [20] also presents the results obtained using the new BCM, where it shows the same precision as the new BNM.

The comparison between the conventional method and the semi-analytic method is given in terms of the results from Tables 2–4 and Fig. 7 of the above two examples. The results of the displacements obtained

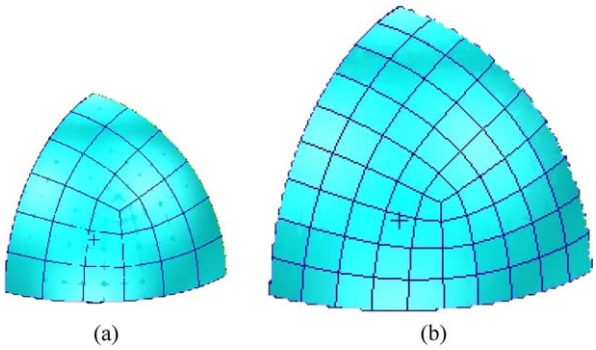

Fig. 6. Meshes of the hollow sphere. (a) Meshes on inner surface; (b) Meshes on outer surface.

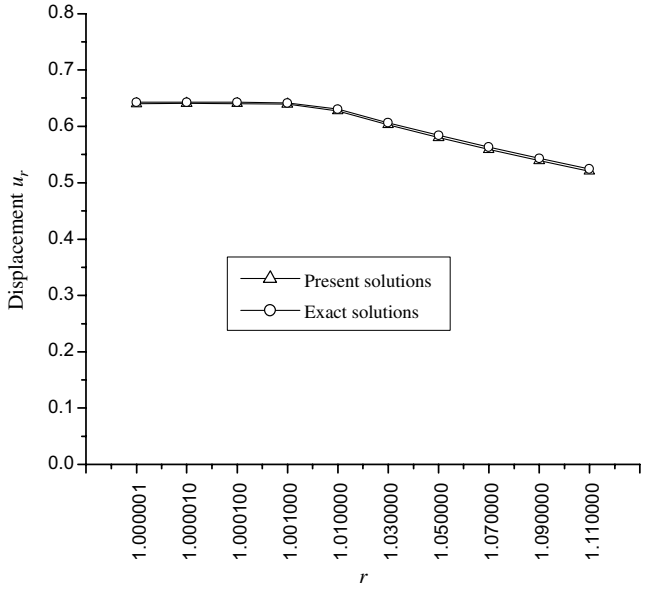

Fig. 7. Radial displacements at the interior points very close to the inner surface.

using the conventional method gradually get degenerative where $e_1 < 0.03$, and ones of the stresses are out of true where $e_1 < 0.1$. The stresses obtained by the semi-analytical method show no signs of deterioration when e_1 reaches 0.001, and the displacements have been excellent agreement with the exact solutions even if e_1 reaches 1×10^{-6}. Therefore the present method, in contrast with the conventional method, reduces the relative distance e_1 by two orders of magnitude within efficient extent of the evaluation of the stresses with the nearly hypersingular integrals in the BEM. The nearly strong singularity, at least, in the range of $e_1 \geqslant 1 \times 10^{-6}$ has been eliminated by the present method.

Table 4 and Fig. 7 show that the semi-analytic method successfully computes the stresses at the interior points in the range of $1.001 \leqslant r$ (implying $r \leqslant 3.999$) and the displacements (with the nearly strongly singular integrals) in $1.000001 \leqslant r$ (implying $r \leqslant 3.999999$) for the hollow sphere, whereas the new BNM and new BCM of Ref. [20] only give the results of the displacements and stresses in $1.01 \leqslant r \leqslant 3.99$. Therefore,

Table 4
Radial and hoop stresses at the interior points very close to the inner surface

Radius (r)	Relative distance e_1	σ_{rr}				$\sigma_{\theta\theta}$			
		Conventional BEM	Present BEM	BNM [20]	Exact solution	Conventional BEM	Present BEM	BNM [20]	Exact solution
1.001	0.002687	×	−1.04880	–	−0.996958	×	0.450990	–	0.522289
1.002	0.005374	×	−1.07239	–	−0.993929	×	0.483642	–	0.520774
1.003	0.008062	×	−1.06975	–	−0.990912	×	0.494724	–	0.519265
1.004	0.010749	×	−1.06288	–	−0.987906	×	0.500010	–	0.517763
1.005	0.013436	×	−1.05523	–	−0.984913	×	0.502832	–	0.516266
1.006	0.016123	×	−1.04763	–	−0.981932	×	0.504354	–	0.514775
1.007	0.018810	×	−1.04031	–	−0.978962	×	0.505100	–	0.513290
1.008	0.021497	×	−1.03334	–	−0.976004	×	0.505338	–	0.511812
1.009	0.024185	×	−1.02669	–	−0.973058	×	0.505227	–	0.510338
1.01	0.026872	×	−1.02035	−0.98020	−0.970123	×	0.504864	0.51168	0.508871
1.03	0.080615	×	−0.928586	−0.92753	−0.913795	×	0.482775	0.49365	0.480707
1.05	0.134359	−0.843312	−0.864060	−0.85789	−0.861676	0.475300	0.456931	0.46201	0.454648
1.07	0.188102	−0.758970	−0.810419	−0.79589	−0.813382	0.412212	0.432513	0.42834	0.430501
1.09	0.241846	−0.759272	−0.763181	−0.74915	−0.768567	0.403907	0.409869	0.40084	0.408093
1.11	0.295589	−0.727359	−0.727359	−0.71229	−0.726925	0.387109	0.387109	0.37928	0.387272

the present method can efficiently calculate the nearly strongly and hypersingular integrals with smaller relative distance e_1 than the new BNM and new BCM, based on a similar mesh pattern.

Example 4 (An ellipsoidal vessel with non-uniform thickness and under internal pressure p). The inner surface of the ellipsoidal vessel is a sphere with radius a. The outer surface is an ellipsoid where the short axis is c along the y-direction and the long axis d along the x- and z-directions, as shown in Fig. 8. The ratio of d/a is fixed at 1.2, while the ratio of c/a is taken as 1.05, 1.03 and 1.01, respectively. For the material, $E = 1$ and $\upsilon = 0.25$. The wall of vessel is so thin near point A that the nearly singular integrals arise in the BE approach. Liu [15] has solved the example by the BEM with removing the nearly strongly singular integrals. Alternatively, the present paper employs the semi-analytical algorithm to calculate this problem. Because of symmetry, only one-eighth of the vessel is meshed in the BEM. Both inner and outer surfaces in one octant are discretized, respectively, with 27 eight-node quadrilateral elements (a total of 54 elements), as shown in Fig. 9. The hoop stresses at points A and B on the inner surface are given in Table 6, together with the results of the BEM and FEM in Ref. [15]. The BEM of Ref. [15] uses 384 elements for the whole vessel with each octant having 48 elements. The FE analysis with 5120 second-order solid elements for one octant is acted as a contrast solution because no analytical solution is found for the test. In Table 5, it is

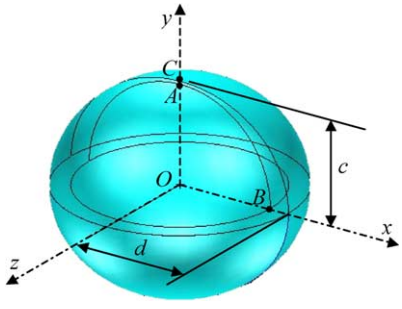

Fig. 8. An ellipsoidal vessel with non-uniform thickness and under internal pressure p.

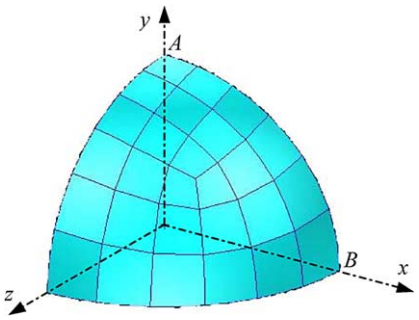

Fig. 9. BEM Meshes on inner or outer surface of the vessel.

Table 5
Hoop stresses ($\times p$) in the ellipsoidal vessel ($d/a = 1.2$)

Ratio c/a	At point A			At point B		
	Present BEM	BEM [15]	FEM [15]	Present BEM	BEM [15]	FEM [15]
1.05	9.759	10.266	9.451	2.938	2.920	3.077
1.03	15.804	15.544	15.691	3.024	2.976	3.164
1.01	40.279	35.098	46.978	3.174	3.145	3.258

seen that the present BEM with the semi-analytical algorithm provides more accurate results than ones of the BEM [15], based on the similar number of elements. Note that for the case of $c/a = 1.01$ the ellipsoidal vessel is very thin at $\overline{AC}$-direction. Actually, the tiny distinction of the geometric model of the BE or FE meshes from the original configuration leads to a great change of the stress field near point A. The results of the present BEM with 54 elements also have some deviation from ones of the FEM at point A for $c/a = 1.01$ (see the last line of Table 5). Here, when a finer mesh with 216 elements is implemented, the present BEM achieves better results (The hoop stress at point A is $45.103 \times p$) for $c/a = 1.01$, as shown in Table 6.

In the other hand, the present method can compute the stresses and displacements in the interior points very close to the boundary. By the use of the semi-analytical algorithm, the results of the stresses along $\overline{AC}$ line in the cases of $c/a = 1.03$ and 1.01 are obtained (see Tables 6 and 7), whereas the BE analysis of Ref. [15] is not available to evaluate the nearly hypersingular integrals. In general, the finite element methods need very many elements to solve this kind of thin-walled problems. It is verified that the BEM with the semi-analytical algorithm can provide accurate solutions for very thin-walled structures.

Table 6
The hoop stresses ($\times p$) at interior points ($c/a = 1.01$, $d/a = 1.2$)

Coordinates			Present BEM (54 elements)	Present BEM (216 elements)	FEM [15] (5120 elements)
x	y	z			
0	1.0	0	40.279	45.103	46.978
0	1.0016667	0	38.1594	46.5412	–
0	1.0033333	0	35.4479	42.5937	–
0	1.005	0	34.0334	40.7967	–
0	1.0066667	0	31.7853	38.1997	–
0	1.0083333	0	24.5039	29.8928	–

Table 7
The hoop stresses σ_{zz} ($\times p$) at interior points ($c/a = 1.03$, $d/a = 1.2$)

Coordinates			Present BEM (54 elements)
x	y	z	
0	1.0	0	15.804
0	1.005	0	15.7712
0	1.01	0	15.4897
0	1.015	0	15.4274
0	1.02	0	15.2922
0	1.025	0	14.3799

5. Conclusions

The concept of the relative distance is proposed in order to describe the influence of the nearly singular integrals in the analysis of three-dimensional BEM. In the present paper, the new semi-analytical algorithm is given to calculate the nearly strongly singular and hypersingular integrals in the BEM. The algorithm is implemented on the linear isoparametric triangular elements and flat elements. By using the technique of the integration by parts, the nearly singular surface integrals are transformed to a series of line integrals along the contour of the elements for which the standard Gaussian quadrature is adequate to obtain very accurate results. Numerical tests demonstrate the considerable effectiveness of the strategy.

For the use of the higher order elements with the curve surface, we suggest the subdivision way utilizing eight triangular elements instead of a quadratic element only when its nearly singular integrals need to be determined. Then the present method is easily implemented for the triangular elements. Of course, the evaluation for the farther elements from the load source can still employ the original methods. With the present algorithm, the displacements and stresses at the interior points very close to the boundary are successfully calculated by the BEM in three-dimensional elasticity problems. Furthermore, the tests show that the BEM can efficiently analyze very thin-walled structures, including the thin laminate structures and coatings. The algorithm does not require any other transformations except for using Eqs. (31), instead of Eq. (23), in comparison with the treatment of the conventional BEM. According to the nature of singularity from Eq. (23) in other physical problems, the present algorithm can also be used to determine the nearly singular integrals in boundary element formulations for such problems.

Acknowledgements

Most of the research work was done while the first author was visiting at the Mathematical Institute A of Stuttgart University, Germany. The first author gratefully acknowledges the support by the Government of Baden-Württemberg and Stuttgart University of Germany, and the National Natural Science Foundation of China (10272039), and thanks Dr. Schulz and Dr. Stainbach of Stuttgart University for many valuable discussions concerning this paper.

References

[1] H.B. Chen, P. Lu, M.G. Huang, F.W. Williams, An effective method for finding values on and near boundaries in the elastic BEM, Comput. Struct. 69 (4) (1998) 421–431.
[2] X.L. Chen, Y.J. Liu, Thermal stress analysis of multi-layer thin films and coatings by an advanced boundary element method, CMES 2 (3) (2001) 337–349.

[3] J.T. Chen, H.K. Hong, Review of dual boundary element methods with emphasis on hypersingular integrals and divergent series, Appl. Mech. Rev. 52 (1) (1999) 17–33.
[4] T.A. Cruse, An improved boundary-integral equation method for three dimensional elastic stress analysis, Comput. Struct. 4 (1974) 741–754.
[5] T.A. Cruse, J.D. Richardson, Non-singular somigliana stress identities in elasticity, Int. J. Numer. Methods Engrg. 39 (1996) 3273–3304.
[6] K. Davey, M.T.A. Rasgado, I. Rosindale, The 3-D elastodynamic boundary element method: Semi-analytical integration for linear isoparametric triangular elements, Int. J. Numer. Methods Engrg. 44 (1999) 1031–1054.
[7] M.G. Duffy, Quadrature over a pyramid or cube of integrals with a singularity at a vertex, SIAM J. Numer. Anal. 19 (6) (1982) 1260–1262.
[8] C. Fiedler, On the calculation of boundary stress with the somigliana stress identity, Int. J. Numer. Methods Engrg. 38 (1995) 3275–3295.
[9] N. Ghosh, H. Rajiyah, S. Ghosh, S. Mukherjee, A new boundary element method formulation for linear elasticity, J. Appl. Mech. 53 (1) (1986) 69–76.
[10] M. Guiggiani, A. Gigante, A general algorithm for multidimensional Cauchy principal value integrals in the BEM, J. Appl. Mech. 57 (4) (1990) 906–915.
[11] M. Guiggiani, G. Krishnasamy, T.J. Rudolphi, F.T. Rizzo, A general algorithm for the numerical solution of hypersingular BEM, J. Appl. Mech. 59 (3) (1992) 604–614.
[12] R. Kieser, C. Schwab, W.L. Wendland, Numerical evaluation of singular and finite-part integrals on curved surfaces using symbolic manipulation, Computing 49 (1992) 279–301.
[13] N.R. Kouitat, J.V. Stebut, Boundary element numerical modeling as a surface engineering tool: application to very thin coatings, Surf. Coatings Technol. 116–119 (1999) 573–579.
[14] J.C. Lachat, J.O. Watson, Effective numerical treatment of boundary integral equation: a formulation for elastostatics, Int. J. Numer. Methods Engrg. 21 (1976) 211–228.
[15] Y.J. Liu, Analysis of shell-like structures by the boundary element method based on 3-D elasticity: formulation and verification, Int. J. Numer. Methods Engrg. 41 (1998) 541–558.
[16] Y.J. Liu, H. Fan, On the conventional boundary integral equation formulation for piezoelectric solids with defects or of thin shapes, Eng. Anal. Bound. Elem. 25 (2001) 77–91.
[17] Y.J. Liu, H. Fan, Analysis of thin piezoelectric solids by the boundary element method, Comput. Methods Appl. Engrg. 191 (2002) 2297–2315.
[18] J. Milroy, S. Hinduja, K. Davey, The elastostatic three-dimensional boundary element method analytical integration for linear isoparametric triangular elements, Appl. Math. Model. 21 (1997) 763–782.
[19] Y.X. Mukherjee, S. Mukherjee, The boundary node method for potential problems, Int. J. Numer. Methods Engrg. 40 (1997) 797–815.
[20] S. Mukherjee, M.K. Chati, X.L. Shi, Evaluation of nearly singular integrals in boundary element contour and node methods for three-dimensional linear elasticity, Int. J. Solids Struct. 37 (2000) 7633–7654.
[21] A. Nagarajan, S. Mukherjee, E.D. Lutz, The boundary contour method of three-dimensional linear elasticity, ASME J. Appl. Mech. 63 (1996) 278–286.
[22] V. Sladak, J. Sladek, On a new BEM formulation for 3D problems in liner elasticity, Eng. Anal. Bound. Elem. 9 (1992) 273–275.
[23] M. Tanaka, V. Sladek, J. Sladek, Regularization techniques applied to BEM, Appl. Mech. Rev. 47 (10) (1994) 457–499.
[24] Y.C. Wang, H.Q. Li, H.B. Cheng, Y. Wu, Calculating the stresses and displacements at arbitrary points with the particular solution field method, Acta Mech. Sin. 26 (2) (1994) 222–231.
[25] W.L. Wendland, H. Schulz, C.H. Schwab, On the computation of derivatives up to the boundary and recovery techniques in BEM, in: IUTAM Symposium of Discretization Methods in Structural Mechanics, Kluwer Academic Publishers, 1999, pp. 155–164.